Nanoscale

PAPER

View Article Online
View Journal | View Issue

Cite this: *Nanoscale*, 2016, **8**, 3376

Intrinsic fluorescence of selenium nanoparticles for cellular imaging applications†

A. Khalid,*[a] Phong A. Tran,*[b,c] Romina Norello,[a] David A. Simpson,[a] Andrea J. O'Connor[b] and Snjezana Tomljenovic-Hanic*[a]

Received 10th December 2015,
Accepted 8th January 2016

DOI: 10.1039/c5nr08771f

www.rsc.org/nanoscale

Nanoparticles hold great potential in contributing to high-resolution bioimaging as well as for biomedical applications. Although, selenium (Se) nanoparticles (NPs) have been investigated owing to their potential roles in therapeutics, the imaging capability of these NPs has never been explored. This manuscript identifies the intrinsic fluorescence of Se NPs, which is highly beneficial for nanoscale imaging of biological structures. The emission of individual NPs and its evolution with time is explored. The photoluminescence spectra has revealed visible to near infrared emission for Se NPs. The work finally reflects on the role of this intrinsic fluorescence for *in vitro* imaging and tracking in fibroblast cells, without the need of any additional tags. This technique would overcome the limitations of the conventionally used methods of imaging with tagged fluorescent proteins and dyes, preventing possible adverse cellular effects or phototoxicity caused by the added fluorescent moieties.

1. Introduction

The antibacterial properties of metallic and semi-metallic nanoparticles (NPs) have been well explored for many pharmaceutical and biomedical applications.[1,2] For these applications it is essential to detect and track such fluorescent NPs in the cell's environment. Laser-induced fluorescence, a spectroscopic method that uses the optical emission excited by absorption of laser light, is one of the key avenues to understand cellular processes.[3] Fluorescent biomarkers have to satisfy three main criteria: biocompatibility, photostability, and suitable wavelengths of absorbance and fluorescence that differ from the cell's auto-fluorescence. In a biological cell, the presence of components such as collagens and flavins produces fluorescent background signals. These molecules typically absorb light in the range 300–500 nm and fluoresce at 400–550 nm. Therefore it is essential for the imaging probe to absorb light at wavelengths longer than 500 nm and to emit light at wavelengths longer than 600 nm.[4]

Organic dyes and fluorescent proteins, used in commercially available confocal systems, meet some of these requirements but they suffer from photobleaching and blinking, precluding their usage in long-term monitoring.[5] Additionally, the major obstacle in the clinical use of these fluorescent materials remains their toxicity.[6,7] The presence of fluorescent dyes modifies the chemistry of the sample and that may be responsible for induced changes in the properties being monitored and toxicity. Therefore, it is advantageous if the NP's intrinsic fluorescence can be used for tracking without any additional tags. This is feasible for metal NPs, such as silver, gold and semi-metallic elements like selenium (Se). All of these NPs have intrinsic fluorescence and a characteristic spectrum. Even though this fluorescence has been investigated within materials science and plasmonics, their fluorescence in biomedical research is usually neglected and replaced by adding tags such as dyes and fluorescent proteins.

Numerous materials including metals, semiconductors, metal oxides,[8] have been employed recently as fluorescent NPs. Zinc oxide (ZnO) NPs, silver suphide (Ag_2S) quantum dots, nanodiamonds (NDs), gold (Au), silver (Ag) and platinum (Pt) NPs are examples of intrinsically fluorescent nanomaterials that are used for bioimaging applications.

Fluorescent Ag_2S nanoclusters are known to possess tunable bright photoluminescence in red, extending to the near-infrared with high emission efficiency. However these NPs are cytotoxic and require capping in order to be useful for bioimaging.[8] ZnO NPs is also a potential material for bioimaging. Intrinsic emission in the red and infrared is reported for ZnO NPs, however these NPs were found to exhibit a blinking behaviour in their emission, which is not suitable for long term bioimaging applications.[9] Nanodiamonds (NDs)

[a]*School of Physics, University of Melbourne, Parkville, VIC 3010, Australia*
[b]*Department of Chemical and Biomolecular Engineering, University of Melbourne, VIC 3010, Australia*
[c]*Institute of Health and Biomedical Innovation, Queensland University of Technology, Kelvin Grove, QLD, Australia. E-mail: asmak@student.unimelb.edu.au, phong.tran@qut.edu.au, snjezana.thanic@unimelb.edu.au*

†Electronic supplementary information (ESI) available. See DOI: 10.1039/c5nr08771f

have been the focus of research for bioimaging applications owing to the presence of room temperature photostable emission centres, their biocompatibility and high emission efficiency. Although NDs are biocompatible and inert, they are non-degradable *in vivo* and *in vitro*.[10]

The photoluminescence of noble metal NPs such as Au and Ag is also a known phenomenon and has gained interest in the recent years due to the inertness of the two materials. Photoluminescence is reported in Au[11] and Ag NPs[12] in the visible to near-infrared region at room temperature. However, Au NPs also exhibit size dependent cytotoxicity effects,[13] which limits their functionality for biological applications.[14] Similarly Ag NPs are reported to exhibit fluorescence in the visible to near-infrared range, however, the emitted light shows blinking and fluctuations limiting their suitability for long term bioimaging.[12]

Se is a semi-metallic element that belongs to the family of chalcogens.[15] Se is a trace element, naturally found in the body, therefore holds more significance in bioimaging as compared to many other metal and metal oxide NPs. In addition, Se NPs are also antimicrobial,[16] anti-cancer, anti-inflammatory[17,18] and hence in practical applications they can potentially be used as both diagnostic tools (cell labelling) and therapeutic agents at the same time. Se has been recognized as an essential element for cellular function in most mammals.[15,19] On one hand, low level of Se has been associated with poor immune function and cognitive decline. On the other hand, high levels of Se can have adverse consequences such as increasing the risk of type 2 diabetes[19] and prostate cancer[20] in some cases. Recent studies point out that Se has the potential to improve human health in many ways, including improving thyroid function,[21] cancer prevention,[22] capture of heavy metals[23] and antibacterial function for use in orthopaedic applications.[16] Even though the largest worldwide usage of Se is in glass manufacturing, due to its red and pink colour,[15] Se NPs in biomedical research are usually tagged with other fluorescent materials.[15,24]

In this study we have investigated Se NPs intrinsic fluorescence intensities and lifetimes. The NPs have been excited with visible green wavelength of 532 nm laser source. With this excitation, we used a low pass 560 nm filter to suppress all the wavelengths below 560 nm, in order to block the input laser excitation. UV excitation has only been used to measure total emission spectrum of Se NPs (without cells). The characteristic fluorescence of Se NPs was used to track the NPs inside fibroblast cells, and to determine the intracellular dynamics of Se. The suitability of Se NPs for long term imaging was verified by monitoring them in cells. Our study demonstrates the feasibility of label-free Se NP fluorescence based imaging *in vitro*.

2. Materials and methods

2.1 Synthesis of Se and PVA coated Se NPs

Sodium selenite, L-ascorbic acid and polyvinyl alcohol (PVA) were obtained from Sigma Aldrich (Castle Hill, NSW, Australia) and dissolved in Millipore water (18 MΩ cm) to the concentrations of 10 mM, 100 mM and 20 mg ml^{-1} respectively. For aqueous synthesis of polymer coated Se nanoparticles at room temperature, sodium selenite and PVA solutions were mixed with volume ratios of 1 : 1. Ascorbic acid solution was then added to this solution at a volume ratio of 3 : 20. The synthesis solution was mixed and left at room temperature for 2 hours for complete reduction of selenite by ascorbic acid to produce elemental Se. The reaction was monitored using a UV-vis spectrophotometer (Varian Cary 50MPR, Agilent Technologies, Santa Clara, USA). The particles were then washed several times with Millipore water by centrifugation at 10 000 RPM for 30 min and collected for experiments. PVA coated Se NPs were obtained by air-drying the Se NPs solution to a stable weight and re-dispersing in water. Uncoated Se NPs were prepared as above without PVA.

2.2 Structural characterization of NPs

The NPs were imaged using transmission electron microscopy (TEM). For this, a drop of NP suspension was placed on a TEM grid and completely air-dried. NP imaging and selected area electron diffraction (SAED) patterns were obtained with a FEI Tecnai TF20 TEM microscope operating at 200 keV. Particle size and zeta potential were investigated using dynamic light scattering (DLS) with a zeta sizer (Nano ZS, Malvern Instruments, UK).

The chemistry of the NPs was studied using X-ray photoelectron spectroscopy (XPS, VG ESCALAB 220i-XL, VG Scientific) equipped with a monochromatic Al Kα X-ray source, which emitted photon energy of 1486.6 eV at 10 kV and 12 mA. Spectra were obtained at a step size of 1 eV (survey scans) or 0.1 eV (region/high resolution scans).

2.3 Confocal imaging for Se and PVA coated Se NPs

Confocal fluorescence scanning was performed using a customized confocal microscope. A 532 nm frequency doubled Nd:YAG continuous wave laser was used for sample illumination at a power of 100 μW, through a 100×, 0.95 NA objective. The samples (Se NPs alone and PVA coated Se) on the silicon (Si) substrates were mounted on a computer controlled stage facing the objective perpendicularly and equipped with an xyz closed loop positioner with 100 μm travel in each direction and step size resolution of 1 nm. The in-plane optical resolution was approximately 300 nm. The fluorescence from the samples was collected with an avalanche photodetector (APD) in the red to near infrared wavelength range. The emission was filtered by a 560 nm long pass filter to remove the incident beam before being detected.

2.4 Spectral analysis of Se

For spectral measurements, Se NPs were deposited on Si substrate and a 325 nm HeCd laser (Kimmon) with a maximum power of 115 mW was used to excite the ensemble of NPs. The emission was collected with a commercial spectrometer (Reinshaw, Invia Reflex micro-Raman).

2.5 Life time measurement for Se NPs

The fluorescence lifetimes of the synthesised Se NPs were characterised using a pulsed laser source and a time correlated photon counting technique. The pulsed green excitation source was constructed from a 520 nm pigtailed laser diode

and a Bias-T circuit was used to modulate the diode current using a Thorlabs LDM9LP driver. The measured response time of the diode and photon detection circuity was 1 ns. The fluorescence lifetimes of the Se NPs were measured after immersing the NPs in phosphate buffered saline (PBS) (Sigma Aldrich) and then drop-casting the NPs onto the glass coverslip. The time-dependent distribution of filtered fluorescence was recorded after each excitation pulse.

2.6 Culture of fibroblast cells with NPs

For confocal imaging, Fibroblasts fibroblasts (3T3 fibroblast, ATCC) were seeded in 1 ml CO_2 independent Medium (Life Technologies, supplemented with 10% fetal bovine serum (FBS) and 1% Penicillin Streptomycin (P/S) (all obtained from Sigma Aldrich) onto the glass cover slips in the wells of a 24 well tissue culture plate at a density of 2500 cells per well. After 24 hours of culture in an incubator (37 °C), each well had Se NP solution added to a final concentration of 100 μg ml^{-1}. The plate was returned to the incubator for another 24 hours for the Se NPs to interact with the cells. After this time period, PBS was used to wash the cells on the glass coverslips in the wells to remove free NPs. Fresh culture medium was added to each well for subsequent wide-field imaging of adherent cells on the glass coverslips.

2.7 Wide-field *in vitro* imaging

Wide-field imaging was performed with a commercial fluorescence microscope (Nikon, Eclipse Ti-U), using a 532 nm Verdi laser operating with a typical power density of 30 W mm^{-2} in a temperature controlled environment of 37 °C. A 5× beam expander was used to expand the excitation beam to 10 mm diameter before focusing the excitation light onto the back aperture of the 100×, 1.45 NA (Nikon) oil immersion objective through a dichroic mirror (Semrock-Di02-R561–25 × 36). A focusing lens (f = 300 mm) focused the excitation light onto the back aperture of the objective creating a uniform wide-field illumination. The laser power P = 140 mW was spread over 80 × 80 μm^2 area and the wide-field fluorescence image was detected with an sCMOS camera (Andor, Neo).[25] The setup[26] was also equipped with the white light microscope that was first used to find a particular area of interest on the sample. The laser was then turned on to image the fluorescence scan for the particular area. Fluorescence imaging of the Se NPs was performed several microns above the surface of the coverglass where the fluorescent Se NPs came into focus. Care was taken to ensure the focal point did not exceed the average height of the cultured cells to make sure that only the NPs inside the cells are being imaged.

3. Results

In section 3.1 the structural characterization of in-house prepared Se NPs is presented. Then, in section 3.2, the absorption and emission spectra of Se NPs are provided. The NPs intrinsic fluorescence is characterized using confocal microscopy and their lifetimes are measured in section 3.3 and 3.4 respectively. The results on the wide-field imaging of Se NPs only are presented in section 3.5. In section 3.6, the Se NPs cultured in the fibroblast cells are tracked and monitored using their intrinsic fluorescence. The photostability of Se NPs and their interactions with cells is tested *in vitro* and discussed in section 3.7. In section 3.8, intracellular dynamics of Se NPs are explored. Finally, in section 3.9 the fluorescence of polymer coated Se NPs is investigated.

3.1 Structural characterization of NPs

The particles imaged using TEM and SAED are shown in Fig. 1 (a)–(c). TEM and high resolution TEM images in Fig. 1(a) and

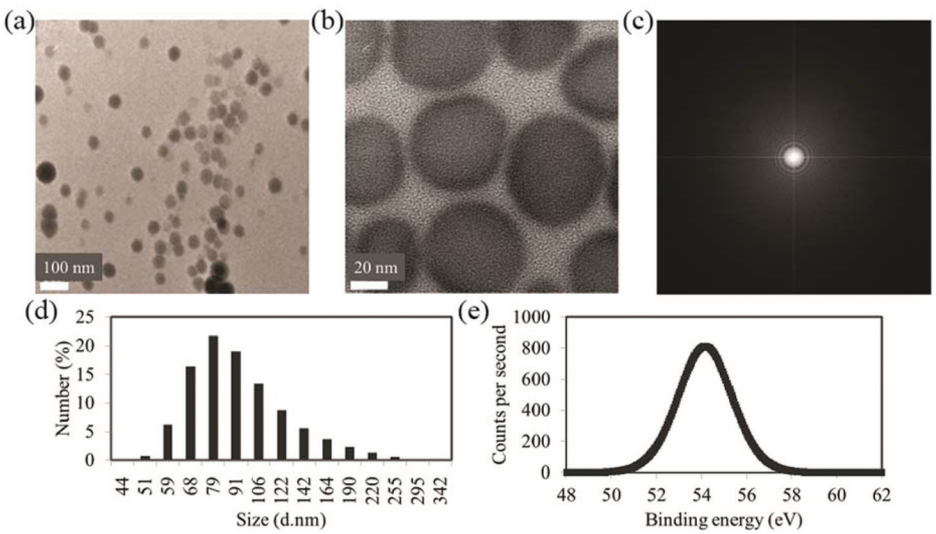

Fig. 1 Characterization of Se nanoparticles *via* (a) TEM and (b) high resolution TEM, showing relatively mono-dispersed particles with sizes of approximately 50 nm. (c) SAED result showing the amorphous nature of Se NPs. (d) Dynamic light scattering measurement presenting size distribution of the NPs in suspension with mean diameter of approximately 80 nm. (e) XPS analysis revealing the binding energy of 54.16 eV for Se 3d peak indicating zero oxidation state of Se after coating with PVA.

(b) together with SAED pattern of Fig. 1(c) indicate the amorphous nature of Se NPs.[27,28] The amorphous elemental Se materials are reported by several groups using similar or slightly different synthesis methods.[29,30]

Particle size and zeta potential are investigated using DLS. As shown in Fig. 1(d), the size distribution measured with DLS shows relatively mono-dispersed NP solution with the majority of particles having sizes of approximately 80 nm. The hydrodynamic sizes of the particles are slightly larger than the sizes determined from TEM images as expected from the limitation of DLS. Larger sizes also exist most likely due to NP aggregations.

The zeta potential value of −24 mV for the NPs is expected to contribute to the stabilization of the NPs in the solution due to electrostatic repulsion between the particles.

From the XPS result of Fig. 1(e), an important characteristic of the surface chemistry of the Se NPs after coating with PVA can be inferred. Uncharged elemental Se has a 3d peak at 55.3 eV.[27,28] The peak shifts to lower binding energy in the figure indicating the interaction of Se with PVA (during synthesis). In previous reports, PVA is shown to act as both an electron donor and a protecting polymer in other NP systems.[31] In our study it is highly likely that PVA bound to the surface of Se and the electron transfer have caused a shift in the binding energy of Se NPs as observed in the XPS graph of Fig. 1(e).

3.2 Absorption and emission spectra

As mentioned in the introduction, red fluorescence is characteristic of numerous types of NPs when illuminated with a green 532 nm laser, such as NDs,[32] metal oxide NPs[9] and noble metal NPs. Each type of NPs has their characteristic absorption and emission band. Here in this section, the absorption and fluorescence emission spectra of Se NPs are investigated.

The measured absorption band for Se NPs is shown with the blue trace in Fig. 2. The absorption is steeply increasing from below λ = 600 nm. The emission spectrum from an ensemble of Se NPs pumped at 350 nm is plotted with red trace in Fig. 2. The UV excitation has been used solely for this part of manuscript in order to observe the full photoluminescence spectrum of Se NPs in the visible to infrared range. The photoluminescence spectrum ranging from 400 nm to 700 nm, shows peak intensity at 416 nm and a maximum intensity broad band between 500–700 nm. The spectrum's intensity has a maximum at 580 nm in the visible to near-infrared wavelength range. This is consistent with the photoluminescence spectra previously reported for annealed Se NPs in PVA films,[33] when excited with 457.9 nm laser.

According to the absorption band any laser excitation below 600 nm would result in emission. However, as mentioned in the introduction, it is essential for the probe to absorb light at wavelengths longer than 500 nm to avoid the cell's autofluorescence.[34] Hence 532 nm wavelength is selected for optical excitation in all the following parts of the manuscript.

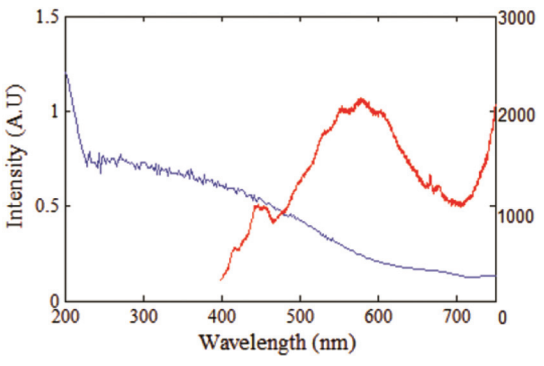

Fig. 2 Measured absorption band (blue), and emission spectrum (red) indicating peak intensities at 416 nm and 580 nm. For the emission spectrum, the NPs have been excited with a UV pump at 325 nm. The intensity scale shown is in arbitrary units (A.U).

3.3 Confocal imaging of Se NPs

The intrinsic fluorescence for individual NPs is reported in this section using near field confocal fluorescence microscopy. The excitation wavelength of 532 nm has been used and the fluorescence collected in red to near infrared detection window of 560–750 nm. Representative confocal image of Se NPs deposited on a Si substrate is shown in Fig. 3(a). The figure shows a 50 × 50 μm^2 coarse fluorescence scan of Se NPs that exhibit red fluorescence when pumped with a green laser.

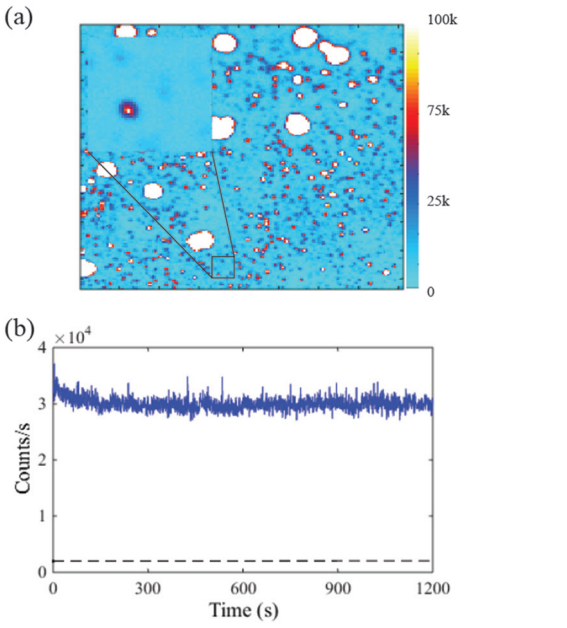

Fig. 3 (a) A 50 × 50 μm^2 near field confocal fluorescence scan (coarse) for Se NPs on the Si substrate. Excitation wavelength of 532 nm is used at an input power of 100 μW. The intensity scale bar is shown to the right of the scan window. The inset shows a fine scan of 5 × 5 μm^2 dimensions. The scan shows distinctively bright Se NP fluorescing with respect to the background. The typical spherical shape of NP is evident from the magnified confocal image in the inset, consistent with the TEM image shown in Fig. 1. (b) Background subtracted emission for the selected Se NP shown in the inset of (a). The dashed line indicates the low background counts from Si substrate.

The scan shows smaller NPs with red center as well as the bigger agglomerated NPs in white with saturated counts. The background fluorescence (light blue) is very low, of the order of 3 kcounts per s, enabling clear identification of Se NPs. The fluorescence of NPs is clearly distinguishable even at a low input power of 100 μW.

The inset of Fig. 3(a) shows a representative 5 × 5 μm^2 fine scan area selected from the coarse scan to determine the emission characteristics of the NPs individually. Fig. 3(b) shows the emission counts, for the NP shown in the inset, as a function of time. The counts recorded for 20 minutes average around 30 kcounts per s and are shown by the blue trace of Fig. 3(b). The general trend of background subtracted emission counts for 10 Se NPs, determined with respect to time showed that initially higher counts reduced and then stabilized to a particular value after a few seconds. The average stable emission counts from a distribution of Se NPs are found to exist in a range of 10–30 kcounts per s.

This level of emission is comparable to the typical emission of non-irradiated NDs.[35] The relatively modest emission comes from the fact that the emitters in both materials are encapsulated in the high refractive index NPs. The refractive index of Se, in the visible range, at the wavelength of λ = 532 nm is n = 3.07 and the refractive index of diamond at the same wavelength is n = 2.42.

This reduction in the counts for NP encapsulated emitter as compared to the emitter radiating alone in air can be calculated analytically[36] and numerically as reported in already published work.[37]

The reduction in counts that comes from NP encapsulation, can be compensated by polymer coating of the NPs with a higher than air refractive index (n = 1). Polymer coating[35] is known to enhance the fluorescence by reducing the refractive index difference between the NP and the coating. The experimental and numerical discussion for polymer coated Se NPs is presented later in the manuscript.

3.4 Lifetime measurement of Se NPs

Fluorescence lifetime, which is the intrinsic property of an emitter is presented for Se NPs, using the time domain data acquisition method. The measured signal can be described well by the single exponential fit.

$$I(t) = I_0 e^{-\tau/t} \quad (1)$$

where I_0 is the intensity at time t = 0, t is the temporal delay with respect to the pump pulse. τ is the fluorescence lifetime, which is the time required by the excited population to decrease exponentially to I_0/e *via* radiative or non-radiative pathways. The average lifetime measured from five Se NPs immersed in PBS is found to be 4.53 ± 0.77 ns. This relatively short fluorescence lifetime suggests that these particles may also be used as a bio-marker for fluorescence lifetime microscopy (FLIM).

3.5 Wide field imaging of NPs

Fluorescent properties of ensemble of NPs, investigated using wide-field imaging are reported in this section. Wide-field imaging illuminated the whole sample with the 532 nm green laser beam and the near infrared fluorescence contribution from each of the illuminated NPs has been measured by selecting the region of interest around that NP.

Fig. 4(a) and (b) show white light microscopic image and wide-field fluorescence images respectively, recorded with Se NPs suspended in PBS. The central fluorescing part of Fig. 4(a) is apparent in the circular bright region of Fig. 4(b), distributed with bright dots, representing the fluorescence from the NPs.

Fig. 4(c) shows time evolution of fluorescence for two of the individual NPs from Fig. 4(b). The average count rate shows the same trend as for individual NPs observed with near-field confocal imaging in section 3.3. Initially higher counts decrease and stabilize after few minutes of recording.

3.6 Wide-field imaging of NPs uptaken by cells

In this section, the incorporation of the NPs into a fibroblast cell is explored and the emission properties of the Se NPs in a biological environment are examined. Application of these NPs as cellular markers on their own without additional tags is hence demonstrated here with wide-field microscopy.

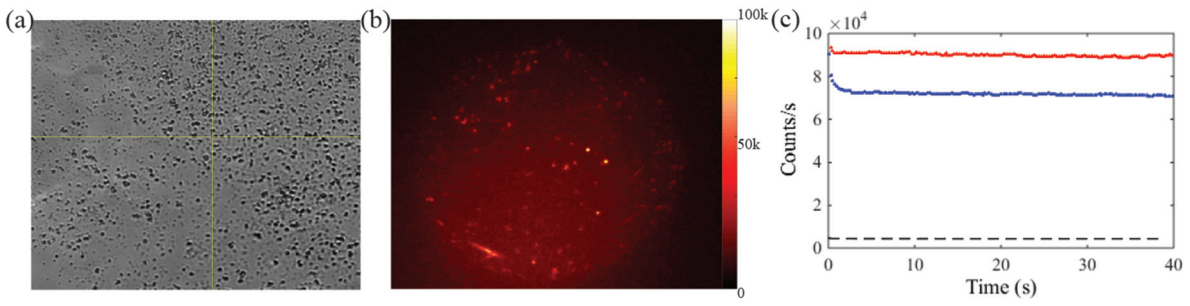

Fig. 4 (a) Wide-field imaging analysis for the 100 times diluted as prepared Se NPs in PBS (a) bright-field image and (b) wide-field fluorescence scan with Se NPs illuminating as bright spots in darker background. (c) Emission counts recorded as a function of time for Se NPs in PBS from the fluorescence scan of Fig. 5(b). The dashed line data shows the background from PBS.

The fluorescence intensity from the Se NPs uptaken by the fibroblast cells is also reported as a function of time.

The white light microscopic image for one of the Se-cultured cells is shown in Fig. 5(a). The corresponding fluorescence image for the cell is shown in Fig. 5(b). The fluorescence image clearly reveals Se NPs inside a cell. The dark region of the cell highlights the nucleus where the Se NPs are not expected to permeate the membrane. The emission intensities from four individual Se NPs in the particular cell are plotted in Fig. 5(c).

The fluorescence decay in the first few seconds indicates the bleaching autofluorescence from the cell. The significant decrease in fluorescence in Fig. 5(c) is attributed to cell autofluorescence which diminishes in the first few seconds of exposure. The signal from the Se NPs remains strong after the initial bleaching of the cell auto fluorescence and is consistent both in terms of count rate and stability over time with that reported in section 3.3 and 3.5.

The cells possess autofluorescence due to the naturally occurring proteins. To check this and determine the contribution of cell's autofluorescence to the fluorescence of NPs, the wide-field fluorescence imaging for cells alone is also presented here.

Fig. 6(a) shows the white light microscopic image of one of the representative cells and Fig. 6(b) shows the corresponding fluorescence image. The autofluorescence from the cells is found to be fast decaying in the first 20 s as shown by the fluorescence scan of Fig. 6(c). The emission counts for the whole cells have also been recorded for eight different cells. Fig. 6(d) provides the least and the most bright autofluorescence signal from cells alone sample. The figure shows that the emission rate for the cells ranges from 6–25 kcounts per s. The statistical data has provided a range of 5–15 kcounts per s background autofluorescence from majority of the cells, which when compared to Fig. 5(c), is low enough to provide significant fluorescence contrast for the NPs cultured inside the cells.

3.7 Cell viability and division unaffected by taking up Se NPs

Optical observation of cells treated with Se NPs investigated in this section have shown normal morphology and non-cytotoxicity which is in agreement with our previous results that explored the interaction of Se NPs with fibroblast cells.[38]

Cell viability testing was performed using a MTT-based assay for the Se NPs at 0, 8, 32 and 128 ppm of Se NPs. Cell viability was found to decrease slightly with increasing Se NP concentration. However, even the highest tested concentration (128 ppm Se) showed low toxicity with more than 70% of cells remaining viable compared to the control.[38]

Se in zero oxidation state (*i.e.* elemental Se) in the form of NPs has been studied by a few groups and is found to exhibit very low toxicity.[39–42] This is consistent with the experimental observation for Se NPs reported here.

The process of cell division after Se NPs internalization is also investigated and the effect of Se NPs taken up on the cells is monitored and presented here. In Fig. 7, a Se NP-cultured cell undergoing cell division is tracked with wide-field microscopy.

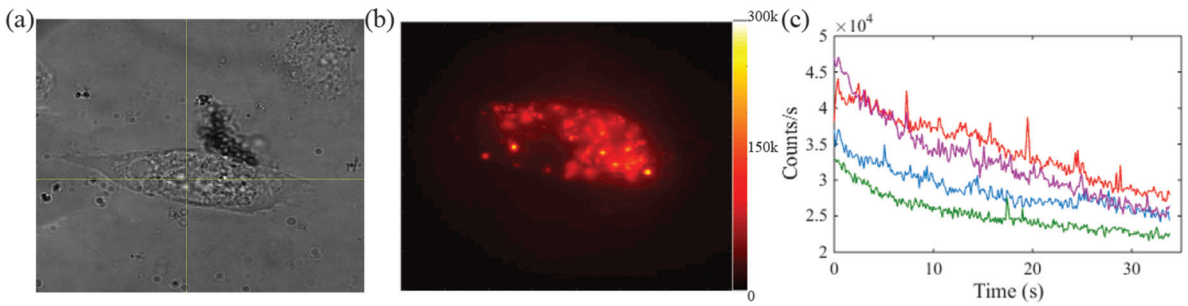

Fig. 5 Se NPs cultured inside fibroblast cells. (a) White light microscopic image of a cell internalized with Se NPs, (b) the corresponding wide-field fluorescence image of cells inside the contour of (a). (c) Emission counts for four Se NPs in cells in (b) plotted as a function of time.

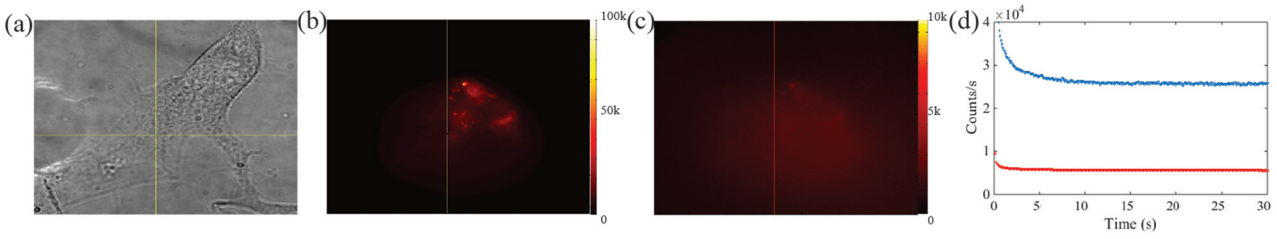

Fig. 6 (a) Bright-field image for cells alone without any NPs. (b) Auto-fluorescence of the fibroblast cells fading away quickly after (c) 20 s time interval. (d) Emission counts plotted as a function of time for the cells only sample.

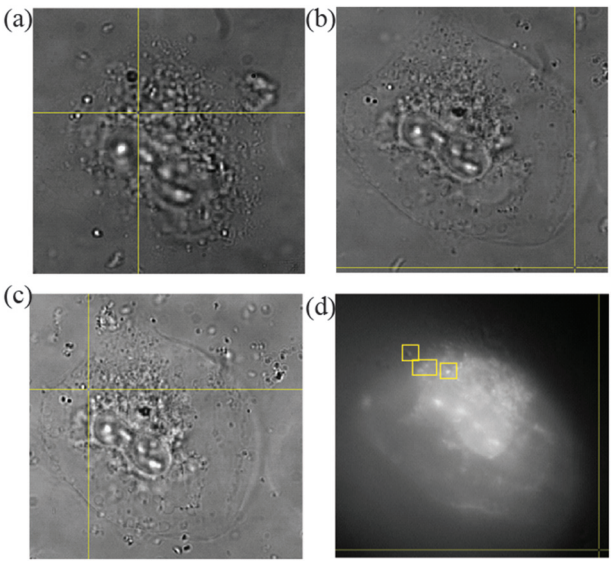

Fig. 7 (a)–(c) Bright-field images of Se cultured cell recorded for 4 hours. Images show scans taken after (a) 0 h, (b) 2 h and (c) 4 h. The cell is under the process of dividing into two daughter cells. (d) The corresponding wide-field fluorescence image of the cell taken after 2 h. The yellow boxes contain the fluorescing Se NPs cultured in cells, used for section 3.8.

Fig. 7(a)–(c) provide the white light microscopic images of the cell within a 4 h period. The process of cell division is unaffected in the presence of Se NPs as the outer cell membrane keeps expanding and contracting with time as is obvious from the respective figures. The corresponding fluorescence image of the Se NP cultured cell is also shown in Fig. 7(d) taken after 2 h of cell monitoring.

The images presented in Fig. 7 are also compared with cells only sample images. The bright field images for a group of cells within a time window of 3 h show similar cell behavior, expansion and contraction of the cell membrane and minimal autofluorescence of the cells (figures provided in the ESI†). This indicates that Se NPs do not alter the cellular processes according to these observations.

3.8 Intracellular dynamics of Se NPs in cells

Section 3.6 shows that the intrinsic fluorescence of Se NPs allows wide-field imaging inside the cells. Observing Se NPs motion inside the cells and the possibility of recording the trajectories of Se NPs in culture cells is demonstrated in this section. After the video processing of the fluorescence images and tracking of Se NP position, the diffusion coefficients (D) have been calculated for four Se NPs (labeled with squares in Fig. 7(d)), using the mean square displacements (r^2) as reported in previous studies.[26,43]

The diffusion coefficient for each of the four Se NPs has been calculated using the slope of the r^2 *versus* time graphs. The following equation has been employed for two dimensional Brownian motion,[44]

$$< r^2 >= 4Dt \quad (2)$$

where t is the time interval over which the measurement is made. The observed linear response of r^2 *versus* time (as shown for one of the NPs in the ESI†) signifies freely mobile, freely diffusing NPs and absence of any driven motion or entrapment of NPs inside the cell membrane. The diffusion coefficient which has been calculated using the slope for the line of best fit (Fig. S1 in ESI†) and is found to vary from 0.001 $\mu m^2\ s^{-1}$ to 0.022 $\mu m^2\ s^{-1}$ for the four NPs. According to the literature,[45] very low diffusion coefficients <0.01 $\mu m^2\ s^{-1}$ are expected for NPs with diameters equal or greater than 50 nm in cells. The D values for Se NPs exist in the range of values published for similar sized NDs.

The quantitative comparison with literature is shown in the Table 1.

Table 1 Comparison of the diffusion coefficient for Se NPs with the already published values for other NPs (with similar size)

	Current work	Ref. 26	Ref. 45	Ref. 46
Diffusion coefficient of bare NPs in cells ($\mu m^2\ s^{-1}$)	70 nm Se NPs: 0.001–0.02	50 nm NDs: 0.054	163 nm NDs: 0.006–0.01	45 nm NDs: 0.003

3.9 Polymer coated Se NPs

Coating Se NPs with a biocompatible polymer ensures their stabilization in solution and is expected to enhance their optical emission properties.[35] The PVA coated Se NPs dispersed in PBS have been found to be stable in PBS. Since the NPs have a relatively high negative surface charge and the PVA polymer is uncharged or weakly negatively charged at pH 7, PVA coated Se NPs are expected to remain stable as the result of both electrostatic interaction and steric hindrance. The solutions of coated Se NPs have been found to be stable for at least one month at room temperature without agglomeration.

According to literature, higher refractive index ($n > 1$) coatings are also known to enhance the emission properties for ND emitters significantly.[35] PVA with a refractive index,[47] n = 1.52 is used in this study to partially coat the Se NPs, which also preserves their antibacterial functionality.[1] The fluorescence properties of the PVA coated Se NPs are investigated in this section and compared with non-coated Se NPs, using confocal imaging.

Fig. 8 shows a 50 × 50 μm^2 coarse confocal scan of the PVA coated NPs pumped with 532 nm at 100 μW. The scan is significantly brighter than the Se only NPs of Fig. 3. The intensity bar on the right of Fig. 8(a) scales to five times brighter counts as compared to Fig. 3(a). The background is significantly low (3 kcounts per s) which distinctly shows the NP fluorescence. A representative fine-scan, 10 × 10 μm^2 in size, for PVA coated

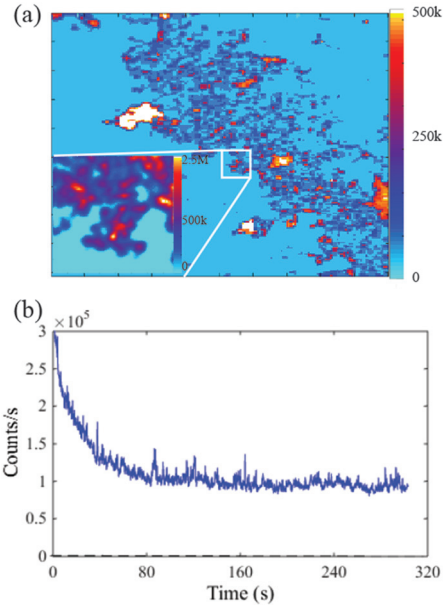

Fig. 8 (a) A 50 × 50 μm^2 confocal fluorescence scan (coarse) of PVA coated Se NPs on Si substrate. An excitation wavelength of 532 nm at an input power of 100 μW is used and the intensity scale bar is shown to the right of the figure. The inset shows a fine scan 10 × 10 μm^2 fluorescence scan for PVA coated Se NPs. (b) Background subtracted emission for the characteristic PVA coated Se NP shown in the inset of (a). Black line at the base represents the low background counts.

NPs is shown in the inset of Fig. 8(a). As compared to Fig. 3(a) inset, the NPs appear to have slightly elongated structure due to the agglomeration of NPs after coating. The intensity bar shows values that go up to millions of counts.

The emission counts for one of the NPs in the inset of Fig. 8(a), recorded *versus* time are presented in the plot shown in Fig. 8(b), where the initially decreasing counts stabilized to 80 kcounts per s.

Compared to Se only NPs, the counts are relatively higher for the PVA coated Se NPs due to the modification of the refractive index.[35] The average increase in emission counts is 2.5–3 times for the polymer coated Se NPs. It is also important to mention here that the emission counts are higher even though the excitation power used for PVA coated Se NPs is kept the same for both coated and non-coated Se NPs.

The increase in counts for the PVA coated NPs is also compared to numerical calculations performed using 3-dimensional Finite-Difference Time-Domain simulations (RSoft FullWAVE).

Emission ratios for PVA coated Se spheres were calculated with respect to Se alone on the Si substrate. The orthogonal and parallel polarizations of the emission dipole are considered relative to the Si substrate.

Table 2 shows the ratio of the emission rates for polymer coated NPs with respect to NPs alone. The emission dipole is assumed to be in the center of the NP and the NP in the center of a spherical PVA coating. Emission ratios in a range of

Table 2 Numerical emission ratios for PVA coated Se NPs spheres with respect to Se NPs alone (deposited on Si substrates). The orthogonal and parallel polarizations are defined with respect to the substrate

Position of emission dipole in PVA coated Se	Orientation of dipole	Sphere size (NP + coating)	Emission ratio
PVA / Se / Si	Orthogonal	100 nm	0.94
		200 nm	1.50
PVA / Se / Si	Parallel	100 nm	1.50
		200 nm	7.80

0.94–1.50 are calculated for 100 nm sphere containing Se NP. For 200 nm sphere, higher emission ratios are found in a range of 1.50–7.80 as given in the Table 2. Thus brighter emission of polymer coated Se NPs can be used if better contrast and brighter emission in bioimaging is needed.

Conclusions

Se NPs are used for a wide range of biomedical applications including anticancer applications and as antibacterial agents. However, their intrinsic fluorescence properties have not been explored for bioimaging. The manuscript reports and discusses for the first time the stable intrinsic fluorescence characteristics of Se NPs. The importance of intrinsic fluorescence of Se NPs is reported in the manuscript which makes them traceable entities inside biological structures. The emission properties of Se NPs with near field confocal microscopy have shown an initial decreasing trend and then the stabilization of counts after a few seconds. The high refractive index of Se results in moderate brightness, as most of the light is trapped inside the high refractive index NP. The Se NPs have been cultured inside the cells and fluorescence tracking of Se NPs in cells has been performed using wide-field imaging. Not only is the fluorescence found to be stable inside the cells, but also the Se NPs are mobile and do not appear to affect the cellular viability or division processes. This implies that the Se NPs can be tracked and imaged in cells, without tags[48] or dyes that are known to chemically modify the biological environment under study. PVA coating around the Se NPs has been found to enhance the emission and this experimental emission enhancement exists inside the range calculated numerically. The dual functionality of Se as an antibacterial material capable of stable fluorescence is highly beneficial for biomedical imaging and therapeutic applications. In conclusion, the manuscript presents imaging (with and without cells) data to support the argument that Se NPs have a distinct fluorescence in the visible to near infrared range, which allows their possible applications for real-time tracking in diagnostic studies.

Acknowledgements

The authors acknowledge Jean-Philippe Tetienne for measuring the lifetime of the Se NPs. This work was partly supported with the assistance of the Australian Research Council (ARC) under Discovery Project Scheme no. DP1096288, University of Melbourne Interdisciplinary Seed Grant, by an award under the Merit Allocation Scheme on the National Facility of the National Computational Infrastructure and CASS Foundation grant. A. K. is partly supported by Melbourne Research Scholarships awarded by The University of Melbourne. P.A.T. is supported by University of Melbourne McKenzie Fellowship. S.T-H. is supported by an ARC Australian Research Fellowship (DP1096288).

Notes and references

1 P. A. Tran and T. J. Webster, *Int. J. Nanomed.*, 2011, **6**, 1553–1558.
2 P. A. Tran and T. J. Webster, *Nanotechnology*, 2013, 24.
3 C. J. Weijer, *Science*, 2003, **300**, 96–100.
4 N. Mohan, Y. K. Tzeng, L. Yang, Y. Y. Chen, Y. Y. Hui, C. Y. Fang and H. C. Chang, *Adv. Mater.*, 2010, **22**, 843–847.
5 L. O. Cinteza, *J. Nanophotonics*, 2010, **4**, 1–37.
6 X. Fei and Y. Gu, *Prog. Nat. Sci.*, 2009, **19**, 1–7.
7 E. C. Jensen, *Anat. Rec.*, 2012, **295**, 2031–2036.
8 O. S. Wolfbeis, *Chem. Soc. Rev.*, 2015, **44**, 4743–4768.
9 A. J. Morfa, B. C. Gibson, M. Karg, T. J. Karle, A. D. Greentree, P. Mulvaney and S. Tomljenovic-Hanic, *Nano Lett.*, 2012, **12**, 949–954.
10 V. N. Mochalin, O. Shenderova, D. Ho and Y. Gogotsi, *Nat. Nanotechnol.*, 2012, **7**, 11–23.
11 T. P. Bigioni, R. L. Whetten and Ö. Dag, *J. Phys. Chem. B*, 2000, **104**, 6983–6986.
12 A. Maali, T. Cardinal and M. Treguer-Delapierre, *Physica E*, 2003, **17**, 559–560.
13 C.-A. J. Lin, T.-Y. Yang, C.-H. Lee, S. H. Huang, R. A. Sperling, M. Zanella, J. K. Li, J.-L. Shen, H.-H. Wang, H.-I. Yeh, W. J. Parak and W. H. Chang, *ACS Nano*, 2009, **3**, 395–401.
14 Y. Pan, S. Neuss, A. Leifert, M. Fischler, F. Wen, U. Simon, G. Schmid, W. Brandau and W. Jahnen-Dechent, *Small*, 2007, **3**, 1941–1949.
15 R. Boyd, *Nat. Chem.*, 2011, **3**, 570–570.
16 P. A. Tran, L. Sarin, R. H. Hurt and T. J. Webster, *Int. J. Nanomed.*, 2010, **5**, 351–358.
17 Y. Y. Huang, L. Z. He, W. Liu, C. D. Fan, W. J. Zheng, Y. S. Wong and T. F. Chen, *Biomaterials*, 2013, **34**, 7106–7116.
18 X. Gao, J. Zhang and L. Zhang, *Adv. Mater.*, 2002, **14**, 290–293.
19 M. P. Rayman, *Lancet*, 2012, **379**, 1256–1268.
20 A. R. Kristal, A. K. Darke, J. S. Morris, C. M. Tangen, P. J. Goodman, I. M. Thompson, F. L. Meyskens, G. E. Goodman, L. M. Minasian, H. L. Parnes, S. M. Lippman and E. A. Klein, *J. Natl. Cancer Inst.*, 2014, **106**, 1–8.
21 L. Schomburg and J. Kohrle, *Mol. Nutr. Food Res.*, 2008, **52**, 1235–1246.
22 D. D. Sun, Y. N. Liu, Q. Q. Yu, X. Y. Qin, L. C. Yang, Y. H. Zhou, L. M. Chen and J. Liu, *Biomaterials*, 2014, **35**, 1572–1583.
23 N. Ralston, *Nat. Nanotechnol.*, 2008, **3**, 527–528.
24 C. R. Song, Q. Fei, H. Y. Shan, G. D. Feng, M. H. Cui, Y. M. Liu and Y. F. Huan, *Spectrochim. Acta Part A*, 2013, **116**, 497–500.
25 D. A. Simpson, A. J. Thompson, M. Kowarsky, N. F. Zeeshan, M. S. Barson, L. T. Hall, Y. Yan, S. Kaufmann, B. C. Johnson, T. Ohshima, F. Caruso, R. E. Scholten, R. B. Saint, M. J. Murray and L. C. Hollenberg, *Biomed. Opt. Express*, 2014, **5**, 1250–1261.
26 A. Khalid, A. N. Mitropoulos, B. Marelli, D. A. Simpson, P. A. Tran, F. G. Omenetto and S. Tomljenovic-Hanic, *ACS Biomater. Sci. Eng.*, 2015, **1**, 1104–1113.
27 M. A. Apecetche, M. Houalla and B. Delmon, *Surf. Interface Anal.*, 1981, **3**, 90–93.
28 C. D. Wagner, W. M. Riggs, L. E. Davis, J. F. Moulder and G. E. Muilenberg, *Handbook of x-ray photoelectron spectroscopy*, Physical Electronics Division, Perkin-Elmer Corp., Eden Prairie, Minnesota, USA, 1979.
29 Z.-H. Lin and C. R. Chris Wang, *Mater. Chem. Phys.*, 2005, **92**, 591–594.
30 B. Pejova and I. Grozdanov, *Appl. Surf. Sci.*, 2001, **177**, 152–157.
31 M. Harada and H. Einaga, *Catal. Commun.*, 2004, **5**, 63–67.
32 A. Khalid, R. Lodin, P. Domachuk, H. Tao, J. E. Moreau, D. L. Kaplan, F. G. Omenetto, B. C. Gibson and S. Tomljenovic-Hanic, *Biomed. Opt. Express*, 2014, **5**, 596–608.
33 A. E. Raevskaya, A. L. Stroyuk, S. Y. Kuchmiy, V. M. Dzhagan, D. R. T. Zahn and S. Schulze, *Solid State Commun.*, 2008, **145**, 288–292.
34 C. Dunsby, J. McGinty and P. French, *Biomedical photonics handbook: Multidimensional fluorescence imaging of biological tissue*, CRC Press, Boca Raton, FL, 2nd edition edn, 2015.
35 A. Khalid, K. Chung, R. Rajasekharan, D. W. Lau, T. J. Karle, B. C. Gibson and S. Tomljenovic-Hanic, *Sci. Rep.*, 2015, **5**, 1–12.
36 H. Chew, *Phys. Rev. A*, 1988, **38**, 3410–3416.
37 K. Chung and S. Tomljenovic-Hanic, *Nanomaterials*, 2015, **5**, 895–905.
38 P. A. Tran, N. O'Brien-Simpson, E. C. Reynolds, N. Pantarat, D. P. Biswas and A. J. O'Connor, *Nanotechnology*, 2015, **27**(4), 1–10.
39 C. Garbisu, S. Gonzalez, W. H. Yang, B. C. Yee, D. L. Carlson, A. Yee, N. R. Smith, R. Otero, B. B. Buchanan and T. Leighton, *BioFactors*, 1995, **5**, 29–37.
40 M. Shakibaie, A. R. Shahverdi, M. A. Faramarzi, G. R. Hassanzadeh, H. R. Rahimi and O. Sabzevari, *Pharm. Biol.*, 2013, **51**, 58–63.

41 J. Zhang, X. Wang and T. Xu, *Toxicol. Sci.*, 2008, **101**, 22–31.
42 H. Wang, J. Zhang and H. Yu, *Free Radical Biol. Med.*, 2007, **42**, 1524–1533.
43 O. Faklaris, D. Garrot, V. Joshi, J. P. Boudou, T. Sauvage, P. A. Curmi and F. Treussart, *J. Eur. Opt. Soc.*, 2009, **4**, 1–18.
44 S. J. B. a. K. M. Blundell, *Concepts in Thermal Physics*, Oxford University Press, Oxford, NewYork, 2011.
45 O. Faklaris, V. Joshi, T. Irinopoulou, P. Tauc, M. Sennour, H. Girard, C. Gesset, J.-C. Arnault, A. Thorel, J.-P. Boudou, P. A. Curmi and F. Treussart, *ACS Nano*, 2009, **3**, 3955–3962.
46 Y. Y. Hui, B. Zhang, Y. C. Chang, C. C. Chang, H. C. Chang, J. H. Hsu, K. Chang and F. H. Chang, *Opt. Express*, 2010, **18**, 5896–5905.
47 P.-f. Xue, J.-b. Wang, Y.-b. Bao, Q.-y. Li and C.-f. Wu, *Chin. J. Polym. Sci.*, 2012, **30**, 652–663.
48 Q. Chen, Q. Yu, Y. Liu, D. Bhavsar, L. Yang, X. Ren, D. Sun, W. Zheng, J. Liu and L. M. Chen, *Nanomedicine*, 2015, **11**, 1773–1784.